FAK phosphorylation at Tyr-925 regulates cross-talk between focal adhesion turnover and cell protrusion

Therese B. Deramaudt, Denis Dujardin, Abdelkader Hamadi, Fanny Noulet, Kaouther Kolli, Jan De Mey, Kenneth Takeda, and Philippe Rondé
Laboratoire de Biophotonique et Pharmacologie, Unité Mixte de Recherche 7213, Centre National de la Recherche Scientifique, and Faculté de Pharmacie, Université de Strasbourg, 67401 Illkirch, France

ABSTRACT **Cell migration is a highly complex process that requires the coordinated formation of membrane protrusion and focal adhesions (FAs). Focal adhesion kinase (FAK), a major signaling component of FAs, is involved in the disassembly process of FAs through phosphorylation and dephosphorylation of its tyrosine residues, but the role of such phosphorylations in nascent FA formation and turnover near the cell front and in cell protrusion is less well understood. In the present study, we demonstrate that, depending on the phosphorylation status of Tyr-925 residue, FAK modulates cell migration via two specific mechanisms. FAK$^{-/-}$ mouse embryonic fibroblasts (MEFs) expressing nonphosphorylatable Y925F-FAK show increased interactions between FAK and unphosphorylated paxillin, which lead to FA stabilization and thus decreased FA turnover and reduced cell migration. Conversely, MEFs expressing phosphomimetic Y925E-FAK display unchanged FA disassembly rates, show increase in phosphorylated paxillin in FAs, and exhibit increased formation of nascent FAs at the cell leading edges. Moreover, Y925E-FAK cells present enhanced cell protrusion together with activation of the p130^{CAS}/Dock180/Rac1 signaling pathway. Together, our results demonstrate that phosphorylation of FAK at Tyr-925 is required for FAK-mediated cell migration and cell protrusion.**

Monitoring Editor
Richard K. Assoian
University of Pennsylvania

Received: Aug 25, 2010
Revised: Dec 15, 2010
Accepted: Jan 20, 2011

INTRODUCTION

Cell migration is implicated in various processes including embryogenesis, tissue regeneration, wound healing, and tumor progression. During this process, cells interact with the microenvironment in part through focal adhesions (FAs). Depending on their state of maturation, FAs may comprise up to 100 structural and signaling molecules that participate in the regulation of FA turnover (Zaidel-Bar *et al.*, 2007a). Migrating cells require that FA formation at the cell front and their disassembly at the cell rear be regulated in a coordinated manner, under the control of distinct molecular signaling pathways (Webb *et al.*, 2004; Iwanicki *et al.*, 2008). Among the multiple signaling molecules contributing to this regulation, FA proteins such as focal adhesion kinase (FAK), Src, paxillin, p130^{CAS}, and ERK play central roles (Cary *et al.*, 1998; Webb *et al.*, 2004). It is now well accepted that regulation of these molecules occurs through tyrosine phosphorylation because interfering with the equilibrium of phosphorylation and dephosphorylation events results in altered cell migration (Zaidel-Bar *et al.*, 2007a). FAK belongs to the group of key molecules responsible for phosphorylation of tyrosines at FAs (Frame, 2004; Schlaepfer and Mitra, 2004). FAK has multiple cellular functions including control of proliferation, survival, cell migration, and adhesion dynamics. Numerous reports have described overexpression, hyperphosphorylation, and/or elevated activity of FAK in a variety of human cancers, including sarcomas, astrocytomas, and carcinomas of the breast, colon, thyroid, prostate, oral cavity, liver, stomach, and ovary (McLean *et al.*, 2005). These highlight a possible key role of FAK in tumorigenesis. It is interesting to note that FAK$^{-/-}$ cells have reduced tyrosine phosphorylation of FA-associated

This article was published online ahead of print in MBoC in Press (http://www.molbiolcell.org/cgi/doi/10.1091/mbc.E10-08-0725) on February 2, 2011.

Address correspondence to: P. Rondé (philippe.ronde@unistra.fr).

Abbreviations used: BSA bovine serum albumin; FA focal adhesion; FAK focal adhesion kinase; FAT focal adhesion targeting; FBS fetal bovine serum; FERM band 4.1–ezrin–radizin–moesin; FRAP fluorescence recovery after photobleaching; GFP green fluorescent protein; Ig immunoglobulin; LED light-emitting diode; MEF mouse embryonic fibroblasts; NA numerical aperture; PBS phosphate-buffered saline; PFA paraformaldehyde; SEM standard error of the mean; TBST Tris-buffered saline with Tween-20; TIRF total internal reflection fluorescence; YFP yellow fluorescent protein.

proteins and display an increased number of larger and more stable FAs compared with normal cells, along with a defect in cell motility due to the inability of cells to initiate FA turnover during cell migration (Ilic *et al.*, 1995; Volberg *et al.*, 2001).

FAK is a ubiquitously expressed nonreceptor cytoplasmic tyrosine kinase consisting of three domains: an N-terminal domain named FERM (erythrocyte band 4.1–ezrin–radizin–moesin), a central kinase domain, and a C-terminal domain termed FRNK (FAK-related nonkinase) including the focal adhesion targeting (FAT) domain and several proline-rich domains. The FERM domain, which mediates direct interaction of FAK with β-integrins (Schaller *et al.*, 1994) and growth factor receptors (Sieg *et al.*, 2000; Carter *et al.*, 2002; Chen and Chen, 2006), has been shown to autoinhibit its activity by directly binding to the kinase domain, thus rendering the latter inaccessible to Src phosphorylation (Cooper *et al.*, 2003; Lietha *et al.*, 2007). Interestingly, FAK binds to the actin-nucleating protein Arp2/3 and promotes its recruitment to nascent adhesions via the FERM domain (Serrels *et al.*, 2007). Thus specific FAK-mediated protein interactions link integrins to the actin-polymerizing cell machinery, thereby facilitating leading edge protrusion. The C-terminal domain interacts with FA-associated proteins including paxillin and talin (Schlaepfer *et al.*, 1994; Schaller and Parsons, 1995), $p130^{CAS}$ (Harte *et al.*, 1996; Tachibana *et al.*, 1997), Grb2 (Schlaepfer *et al.*, 1994), ASAP1 (Liu *et al.*, 2002), and p85α of PI3K (Guinebault *et al.*, 1995). Furthermore, the C-terminal domain is both necessary and sufficient for localization of FAK to FAs.

On integrin engagement with the extracellular matrix, FAK autophosphorylates its Tyr-397 residue, which in turn results in recruitment of Src family kinases and induction of several downstream signaling pathways (Parsons, 2003). Depending on the cell type, Src family kinases or other kinases phosphorylate the remaining tyrosine residues of FAK: Tyr-407, Tyr-576, Tyr-577, Tyr-861, and Tyr-925 (Calalb *et al.*, 1995, 1996; Schlaepfer and Hunter, 1996). Unlike other phosphotyrosine residues, phosphorylation of Tyr-925 residue has been identified as a Src-dependent process because phosphorylation of Tyr-925 is significantly reduced in cells expressing a kinase-defective mutant of Src (Brunton *et al.*, 2005).

The aim of the present study was to assess the effects resulting from phosphorylation of FAK at Tyr-925. We report that depending on the cellular context, FAK phosphorylation at Tyr-925 acts as a switch that coordinates either FA disassembly or the formation of a cell edge protrusion. We used the nonphosphorylatable Y925F-FAK and the phosphomimetic Y925E-FAK mutants to demonstrate the importance of FAK phosphorylation in the regulation of cell migration through activation of the $p130^{CAS}$/Rac1 signaling pathway and induction of cell protrusion. Our findings emphasize the importance of targeting specific phosphorylation sites of FAK, in our case Tyr-925, for therapeutic approaches. Development of such site-specific inhibitors might represent a promising means to prevent tumor metastasis.

RESULTS

Nonphosphorylatable and phosphomimetic mutants of FAK

To investigate how phosphorylation of FAK at Tyr-925 is implicated in FA turnover and cell migration, site-directed mutagenesis was utilized to replace Tyr-925 with either a nonphosphorylatable phenylalanine (Y925F-FAK) or a phosphomimetic glutamic acid (Y925E-FAK). The latter point mutation has been used successfully in other proteins to mimic a constitutive tyrosine phosphorylation environment (Kassenbrock and Anderson, 2004; Tomar *et al.*, 2004; Potter *et al.*, 2005; Zaidel-Bar *et al.*, 2007b). Moreover, several studies analyzing FA dynamics have used Y→E substitution to mimic phosphorylation charges of adhesion proteins (Zaidel-Bar *et al.*, 2007b; Pasapera *et al.*, 2010). Indeed, in the latter study, phosphomimetic mutation of paxillin induced the recruitment of vinculin to the adhesion site. After confirmation of mutations by sequencing, $FAK^{-/-}$ mouse embryonic fibroblasts (MEFs) were transiently transfected with wild-type FAK, Y925F-FAK, or Y925E-FAK. All three proteins were correctly expressed at their expected molecular weights (Figure 1A), with similar global expression levels once normalized to paxillin or the internal loading control (β-actin). FAK was undetectable in control (nontransfected) $FAK^{-/-}$ MEFs (unpublished data). To visualize the loss of phosphorylation at amino acid 925, Western blots were done using an antibody that recognizes phosphorylated Tyr-925. No signal was detected for Y925F-FAK and Y925E-FAK mutants compared with wild-type FAK, thus validating the point mutations at Tyr-925 (Figure 1A). Moreover, phosphorylation of FAK at Tyr-925 is believed to induce conformational changes of the FAT domain (Dixon *et al.*, 2004; Prutzman *et al.*, 2004). Accordingly, while FAK and Y925F-FAK were recognized by the conformation-specific monoclonal 2A7 antibody (Cooley *et al.*, 2000; Prutzman *et al.*, 2004), Y925E-FAK was not (Figure 1B). The effect of mutation of FAK at Tyr-925 on the state of FAK phosphorylation was next investigated. Immunoblotting with phosphospecific FAK antibodies revealed a significant increase in phospho-FAK at Tyr-861 in Y925E-FAK cells compared with Y925F-FAK and wild-type FAK cells

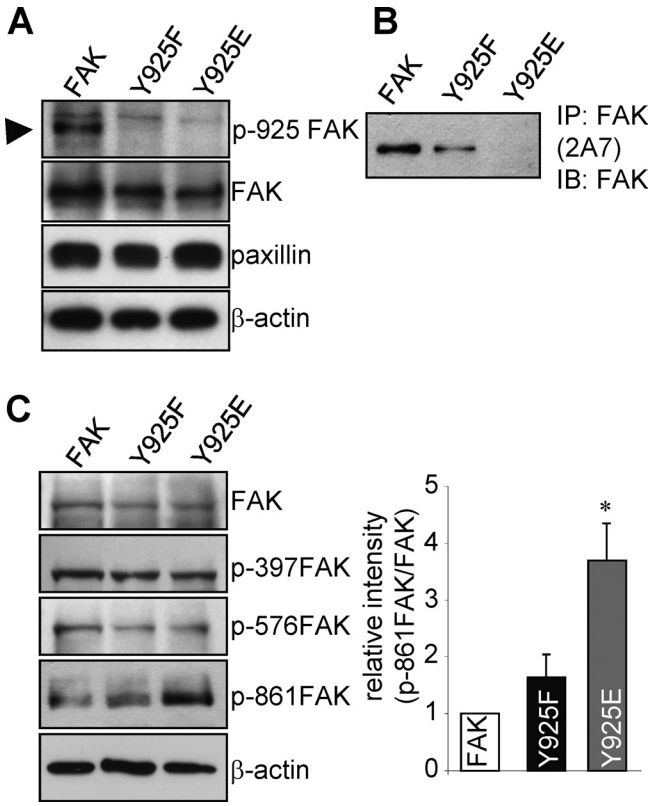

FIGURE 1: Expression of wild-type FAK, Y925F-FAK, and Y925E-FAK. (A) Representative Western blots of phospho-Y925-FAK (p-925 FAK), total FAK, and total paxillin in $FAK^{-/-}$ MEFs transfected with wild-type and mutant FAK. The black arrowhead shows the signal for FAK. (B) Representative blot showing FAK immunoprecipitated by the conformation-specific anti-FAK (2A7 clone) antibody, which binds to native FAK. (C) Western blots showing the phosphorylation status of FAK at Tyr-397, Tyr-576, and Tyr-861 in wild-type FAK, Y925F-FAK, and Y925E-FAK cells. Graph shows increased FAK phosphorylation at Tyr-861 in Y925E-FAK cells compared with wild-type FAK cells. *$p < 0.05$; $n = 3$ independent experiments.

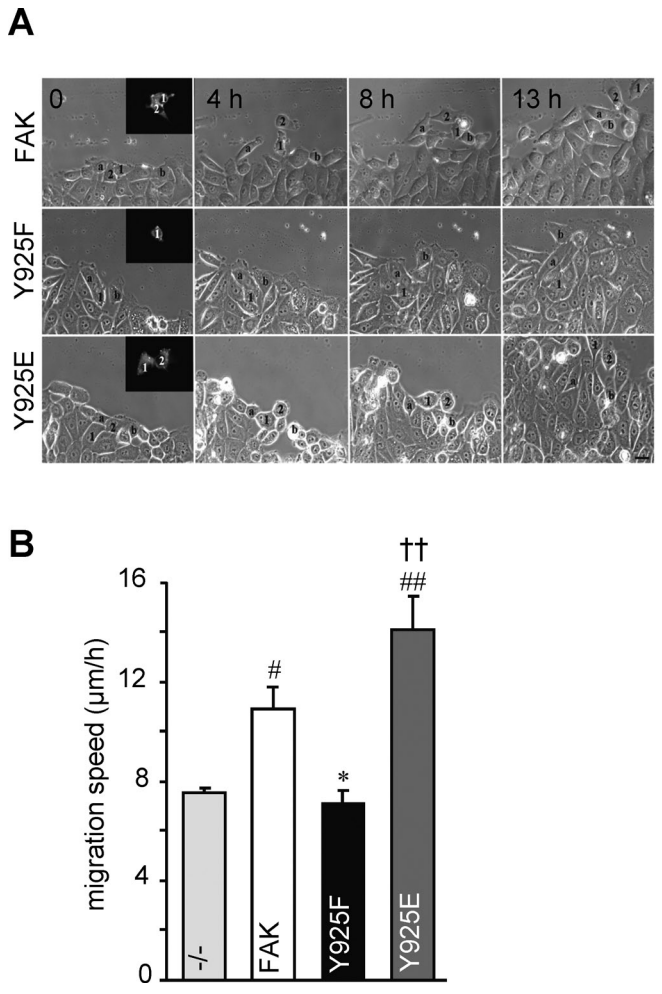

FIGURE 2: Migration of wild-type FAK, Y925F-FAK, and Y925E-FAK cells. (A) After wounding, migrating cells expressing wild-type or mutant fluorescent FAK (see inserts in t = 0 images) were tracked for 13 h. Panels show representative images of migrating cells at the wound leading edge taken after 4, 8, and 13 h. Fluorescent cells are numbered, and nonfluorescent cells are labeled alphabetically. Scale bar, 20 μm. (B) The average migration speed was quantified from the tracking data for control FAK$^{-/-}$ (n = 111), wild-type FAK (n = 14), Y925F-FAK (n = 19), and Y925E-FAK (n = 16) cells. *p < 0.0013 vs. wild-type FAK cells, #p < 0.003 and ##p < 0.0002 vs. control cells, ††p < 0.0002 vs. Y925F-FAK cells.

(Figure 1C) while, in contrast, phosphorylation at Tyr-397 and Tyr-576 was unaffected.

Expression of Y925F-FAK and Y925E-FAK alters cell migration

Wound healing experiments were done to evaluate how Tyr-925 phosphorylation affects cell migration. FAK$^{-/-}$ MEFs as well as MEFs transiently expressing wild-type FAK, Y925F-FAK, and Y925E-FAK were grown to confluence, wounded by scraping with a pipette tip, and tracked for 13 h (Figure 2A). Migration speed of individual cells at the leading edge of the wound was determined for each cell line (Figure 2B). Wild-type FAK cells (10.9 ± 0.88 μm/h) and Y925E-FAK cells (14.1 ± 1.36 μm/h) migrated significantly faster than Y925F-FAK cells (7.13 ± 0.5 μm/h) and control MEFs (7.51 ± 0.23 μm/h). Thus expression of wild-type FAK increased migration speed by 31% compared with control FAK$^{-/-}$ cells, while Y925F-FAK cells had a 34% decrease and Y925E-FAK cells a 22% increase in migration speed compared with wild-type FAK cells (Figure 2B). These data confirm that phosphorylation at Tyr-925 plays a critical role in regulating cell migration.

Phosphorylation of Tyr-925 affects FAK turnover at FAs

Cell motility is dependent on the ability of FAK to disassemble FAs. Disassembly of FAs is correlated to the time residency of several proteins at these sites including FAK (Giannone *et al.*, 2004; Hamadi *et al.*, 2005), zyxin (Lele *et al.*, 2008), vinculin (Mohl *et al.*, 2009), paxillin (Schober *et al.*, 2007), and talin (Millon-Fremillon *et al.*, 2008). To study the effects of Tyr-925 phosphorylation on FA disassembly, the mobility of wild-type FAK and FAK mutants was assessed by fluorescence recovery after photobleaching (FRAP) experiments. The yellow fluorescent protein (YFP) moiety contained in the FAK constructs present in peripheral FAs randomly selected at the periphery of the cells or in the cytosol was photobleached with short high-power 488 nm excitation using a Kr/Ar laser (Figure 3A), and the recovery of fluorescence in the bleached regions was followed by time-lapse imaging over the ensuing 80 and 140 s, in the cytosol and at FAs, respectively (Figure 3B). Recovery of fluorescence after photobleaching at FAs was substantially faster in Y925F-FAK cells ($t_{1/2}$ = 13.2 ± 1.7 s) compared with wild-type FAK ($t_{1/2}$ = 25.6 ± 2.5 s) or Y925E-FAK cells ($t_{1/2}$ = 25.5 ± 1.1 s) but was not different in the cytosol of the three cell lines. The faster recovery of nonphosphorylatable Y925F-FAK at FAs is consistent with phosphorylation of FAK at Tyr-925, contributing to increase the time residency of FAK at FAs and thus in the regulation of FAK turnover.

Phosphorylation of Tyr-925 affects FA disassembly

We previously reported that phosphorylation of FAK at Tyr-397 was implicated in cell migration because expression of nonphosphorylatable Y397F-FAK leads to reduced FA disassembly and decreased cell migration (Hamadi *et al.*, 2005). To characterize the effects of constitutive phosphorylation or dephosphorylation at Tyr-925 on FA disassembly, adhesion dynamics were evaluated. To this purpose, we assessed FA disassembly using FAK kinetics at adhesion sites because the rate constant for disassembly of several FA proteins including paxillin, FAK, and zyxin has been shown to be identical, thus demonstrating that the disassembly of these molecules is concerted rather than sequential (Webb *et al.*, 2004). Nevertheless, in order to validate the use of FAK or FAK mutants as a marker for FA disassembly, we analyzed FAK and vinculin disassembly in cells coexpressing FAK–green fluorescent protein (GFP) and cherry-vinculin, and FAK and vinculin disassembly in cells coexpressing Y925E-FAK-GFP and cherry-vinculin. Our results showed that disassembly of FAK or Y925E-FAK and vinculin occurred simultaneously (Supplemental Figure S1), consistent with the disassembly of these FA proteins being a valid marker of FA dynamics. Therefore FA disassembly of wild-type FAK, Y925F-FAK, and Y925E-FAK cells was assessed by time-lapse confocal microscopy (Figure 4A). Analysis of sequential images shows that cells expressing wild-type FAK and Y925E-FAK have similar dissociation rates, while both cell lines show faster FA dissociation rates compared with that of Y925F-FAK cells. In FAs, fluorescence of wild-type FAK and Y925E-FAK decreased to background level after ~20 min while 30–40 min were required for Y925F-FAK. Calculated extinction rates of fluorescence for wild-type FAK, Y925E-FAK, and Y925F-FAK are $(6.9 \pm 0.2) \times 10^{-2}$ min^{-1}, $(7.8 \pm 0.3) \times 10^{-2}$ min^{-1}, and $(4.2 \pm 0.1) \times 10^{-2}$ min^{-1}, respectively (Figure 4C).

To further study how phosphorylation of Tyr-925 affects the number of FAs displaying dynamic processes, FAs of cells expressing wild-type FAK, Y925F-FAK, or Y925E-FAK were observed for 1 h. Images taken at t = 0 (red) and t = 60 min (green) were superimposed (Figure 4B), and quantification of peripheral FA dynamics

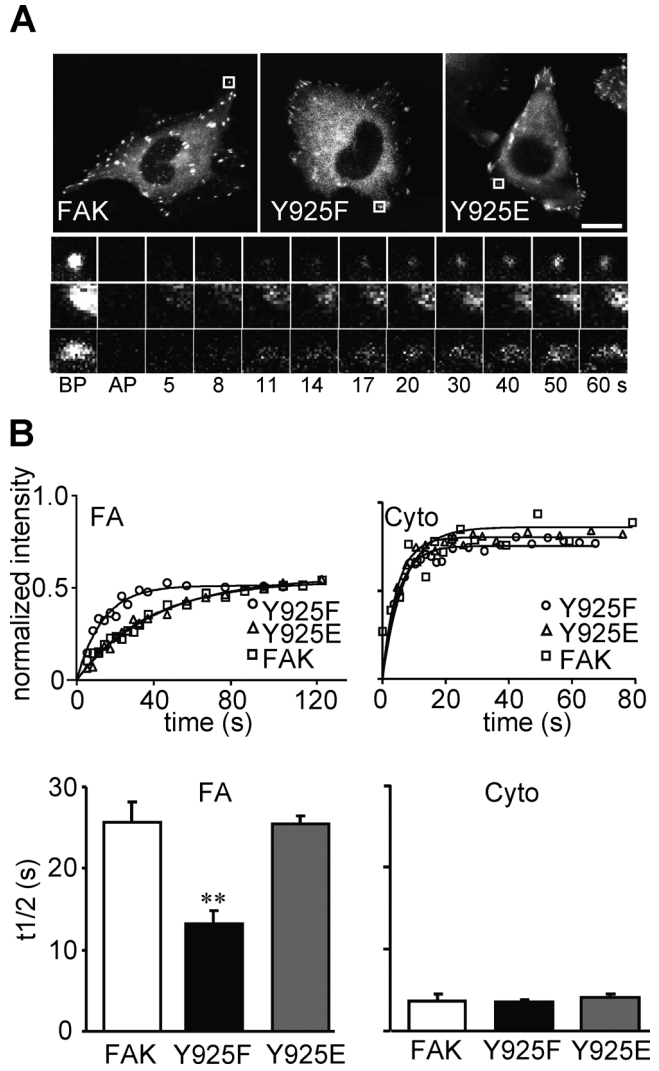

FIGURE 3: Dynamics of fluorescently tagged wild-type FAK, Y925F-FAK, and Y925E-FAK analyzed by FRAP. (A) Images of transiently transfected FAK$^{-/-}$ MEFs show wild-type FAK, Y925F-FAK, and Y925E-FAK at the cell periphery before photobleaching of FAs (boxed areas). Scale bar, 10 μm. The time-lapse sequences below show recovery after bleaching of corresponding FAs. BP, before photobleaching; AP, immediately after photobleaching. Scale bar, 2 μm. (B) Representative examples of fluorescence recovery kinetics for wild-type FAK, Y925F-FAK, and Y925E-FAK at FAs (left) and in the cytosol (right). At FAs, note the significantly shorter recovery half-time for Y925F-FAK compared with Y925E-FAK and wild-type FAK. Mean ± standard error of the mean (SEM) was calculated from n = 17 FAs (wild-type FAK), n = 14 FAs (Y925F-FAK), n = 13 FAs (Y925E-FAK), and 5–7 cytosolic compartments of independent cells. **p < 0.001 vs. wild-type FAK.

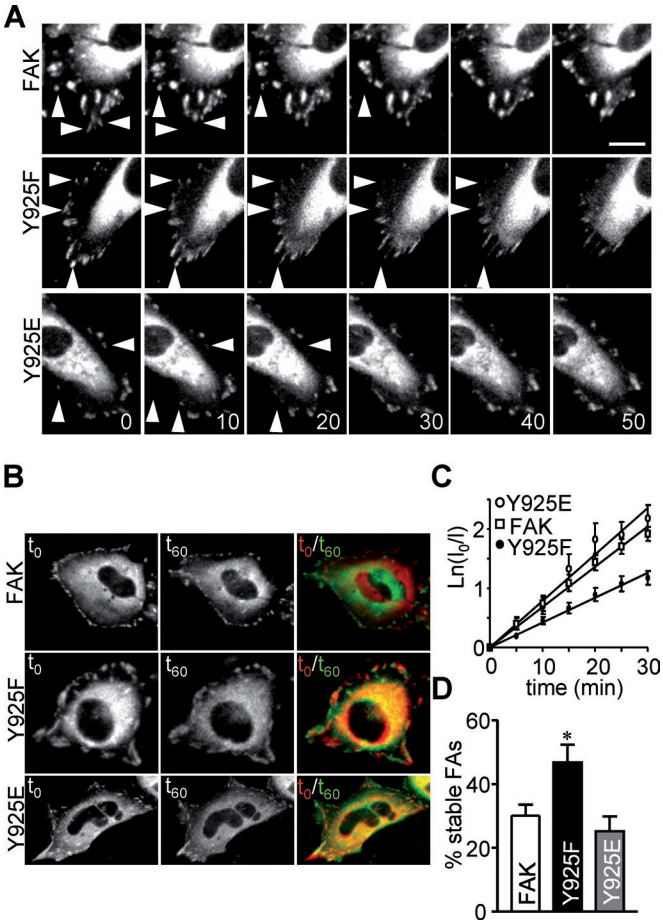

FIGURE 4: Quantification of wild-type FAK, Y925F-FAK, and Y925E-FAK dynamics and FA disassembly. (A) Confocal time-lapse images were taken every 5 min for 1 h; representative images are shown every 10 min. Arrows indicate positions of FAs initially containing wild-type FAK, Y925E-FAK, and Y925F-FAK. Scale bar, 10 μm. (B) Images of cells visualized at t = 0 (left) and at t = 60 min (center). In the time-merged images (t0/t60; right), disassembled FAs appear in red, stable FAs in yellow, and newly formed FAs in green. (C) Time course of FA disassembly in cells from (A) presented as the ratio of integrated fluorescence intensity at FAs relative to initial intensity calculated every 5 min; mean ± SEM calculated for wild-type FAK (n = 47 FAs), Y925F-FAK (n = 39 FAs), and Y925E-FAK (n = 36 FAs). Rate constants of FA disassembly were calculated from the slopes of the lines. (D) Percentages of stable FAs were calculated from images in (B) as the number of FAs in wild-type FAK, Y925F-FAK, and Y925E-FAK cells at t = 60 min compared with t = 0. Mean ± SEM, six cells from independent experiments. **p < 0.05 vs. wild-type FAK cells.

show a 36% increase in the number of stable FAs in Y925F-FAK cells compared with wild-type FAK and Y925E-FAK cells. Interestingly, the percentage of stable FAs in wild-type FAK and Y925E-FAK cells was not different (Figure 4D). Taken together, our results indicate that the phosphorylation status of Tyr-925 contributes to the regulation of FA disassembly and thus to the stability of FAs.

Enhanced cell protrusion in Y925E-FAK cells

It is intriguing to note that FA dissociation rate and FAK turnover in Y925E-FAK cells are comparable to those of wild-type FAK cells, while the migration speed of Y925E-FAK cells is significantly faster (Figure 2). We then analyze the ability of cells expressing our different FAK mutants to undergo protrusion or retraction. The fluorescent signals from our fusion constructs were imaged every 10 min for 1 h. Successive images were superimposed, with t = x represented in red and t = x + 10 min in green (Figure 5A). Newly formed FAs appear in green at leading edges and disassembled FAs in red, with the two colors corresponding to cell protrusion and retraction, respectively. Quantifications of the protrusive-retractile activities at the cell edges of wild-type FAK, Y925F-FAK, and Y925E-FAK cells was carried out for 20-min periods (Figure 5B), according to a method previously described (Grande-Garcia *et al.*, 2007). The

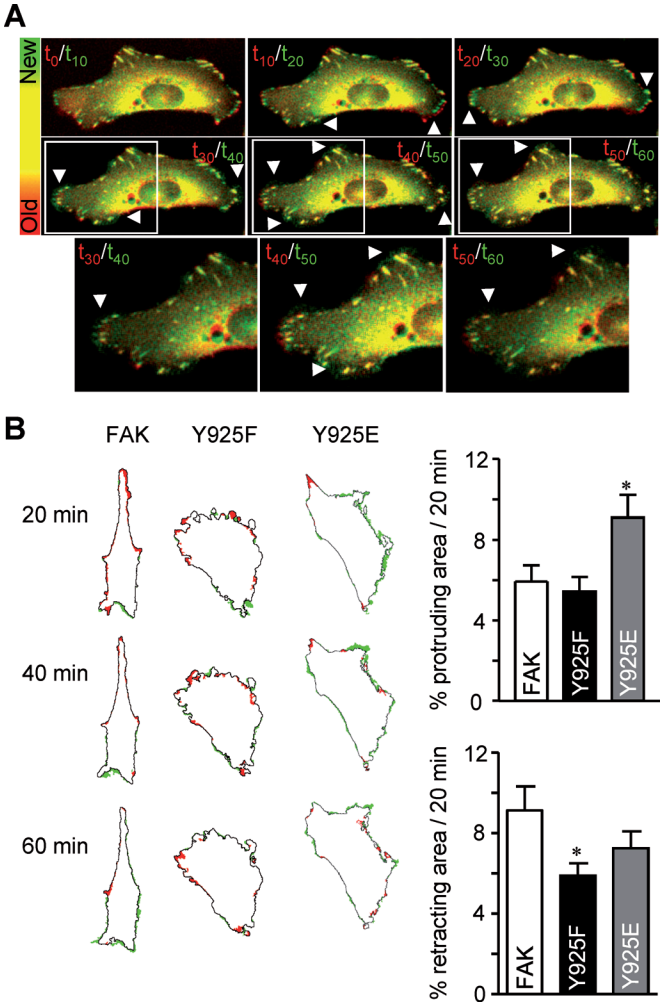

FIGURE 5: Increased cell protrusion in Y925E-FAK cells. (A) Time-lapse confocal microscopy of Y925E-FAK cells for 60 min. Images represent merged confocal images taken at t = x (red) and at t = (x + 10) min (green). Note the presence of multiple protrusions around the cell accompanied by formation of FAs (white arrowheads). Scale bar, 10 μm. (B) Time-lapse videos were used to calculate cell protrusion and retraction areas. Time-merged images of wild-type FAK, Y925F-FAK, and Y925E-FAK cells are shown with protruding edges in green and retracted edges in red. Mean ± SEM of protrusions or retractions over a 20-min period of imaging from wild-type FAK (n = 21 protrusion/retractions), Y925F-FAK (n = 15), and Y925E-FAK (n = 24) cells. *p < 0.05 vs. wild-type FAK cells.

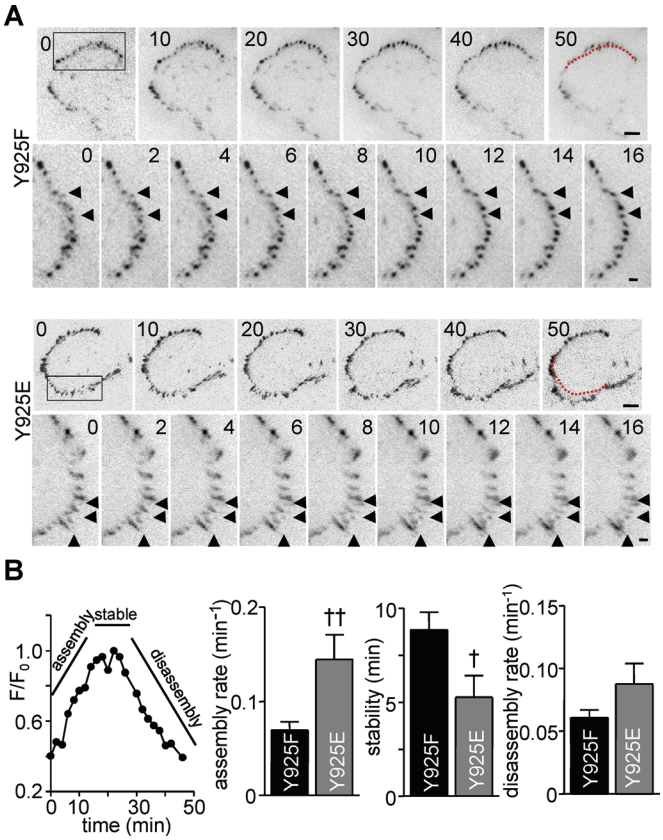

FIGURE 6: TIRF imaging of Y925F-FAK and Y925E-FAK cells. (A) Formation of nascent adhesions in Y925F-FAK and Y925E-FAK cells visualized by TIRF microscopy. Images were acquired at 2-min intervals for 1 h. Images of whole cells are shown at 10-min intervals (scale bar, 5 μm), and images corresponding to the magnification of the boxed areas are shown every 2 min (scale bar, 1 μm). In whole cell images, note the increase in cell protrusion activity in Y925E-FAK cells compared with Y925F-FAK cells (dotted red lines in t = 50 correspond to FAs at the cell edge at t = 0). Arrowheads indicate assembly of nascent adhesions at the cell edge. Note the increase in FA assembly rate in Y925E-FAK cells compared with Y925F-FAK cells. (B) Nascent adhesion lifetime can be resolved into three discrete phases—assembly, stability, and disassembly—by measuring fluorescence intensity with time (left). Rate constants for the assembly and disassembly of nascent adhesions. Mean ± SEM, n = 34 (Y925E-FAK) and 26 (Y925F-FAK) individual FAs.

results show that Y925F-FAK cells had a 35% decrease in retractile activity compared with wild-type FAK cells. Interestingly, Y925E-FAK cells show a 33% increase in formation of cell protrusions compared with wild-type FAK cells.

To analyze in further detail the mechanisms implicated in the formation of cell protrusions, we focused on the adhesion population at leading edges. Because nascent adhesions localized at thin protruding cell edges are barely detectable using conventional confocal microscopy, we used total internal reflection fluorescence (TIRF) microscopy. Previous studies using double-color time-lapse movies visualizing FA proteins such as paxillin and zyxin demonstrated sequential protein recruitment into focal complexes (Zaidel-Bar *et al.*, 2003). We found that FAK is apparently incorporated in protrusive areas before vinculin (Supplemental Figure S2), stressing the importance of analyzing FAK incorporation to evaluate early steps of adhesion formation during protrusion. As illustrated in Figure 6A, an array of punctuate adhesions were observed at the leading edges of Y925F-FAK and Y925E-FAK cells. However, Y925E-FAK cells exhibited prominent protrusions over the 50-min observation period, while Y925F-FAK cells were notably less protrusive (see evolution of the edge compared with the drawn red line at t = 50 for both conditions). Closer examination of the protrusive area of Y925E-FAK cells showed the presence of adhesions that were highly dynamic on a time scale of a few minutes compared with adhesions observed in Y925F-FAK cells (Figure 6A). Analysis by compartmenting the three discrete phases that form the lifetime of dynamic adhesions revealed an increase in assembly rate and a decrease in the stability period in Y925E-FAK compared with Y925F-FAK cells (Figure 6B).

To analyze the relationship between FA dynamics at leading edge and membrane protrusion, we looked at cell protrusion by bright field transmitted with light-emitting diode (LED) illumination microscopy together with TIRF microscopy. Time-lapse acquisition

in dual LED/TIRF mode of Y925F-FAK (LED, Supplemental Video 1; TIRF, Supplemental Video 2; dual LED/TIRF, Supplemental Video 3) and Y925E-FAK cells (LED, Supplemental Video 4; TIRF, Supplemental Video 5; dual LED/TIRF, Supplemental Video 6) showed that newly formed fluorescent nascent FAs were exclusively localized at protruding leading edges (Figure 7A). Arrowheads point to existing or appearing FAs at the leading edge in order to facilitate the tracking of their evolution through time. It is worth noting that some of the FAs (Figure 7A, arrowheads 1 in Y925F and Y925E) start to disassemble when new nascent FAs assemble at their front (Figure 7A, arrowheads 2). Note also that nascent FAs that localized on the sides of the migrating cell tend to mature and stabilize. Kymograph analyses were performed on both TIRF and LED images taken between t = 0 and t = 30 min (Figure 7B). Protrusion speed was obtained by measuring the distance between the two arrows in the kymograph representation. Our results indicated, first, similar rates of membrane protrusion and FA assembly and, second, a significant increase in cell protrusion speed in Y925E-FAK cells (20.13 ± 1.2 μm/h) compared with Y925F-FAK cells (10.24 ± 2.1 μm/h) (Figure 7C). Collectively, these results are consistent with FAK controlling cell migration by regulating the protrusive activities at the leading edges of motile cells.

Because FAK Tyr-925 is a Src-specific substrate (Brunton *et al.*, 2005), we tested whether phosphorylation of this site by constitutively activated Src could mimic some of the effects observed in FAK-Y925E cells. For this purpose, FAK$^{-/-}$ MEFs were cotransfected with either wild-type FAK or Y925F-FAK together with mCherry-Src-Y530F. Our results indicated that constitutively activate Src induces formation of broad and/or multiple lamellipodia in FAK expressed cells but not in Y925F-FAK cells (Supplemental Figure S3). This is in agreement with our previous observation establishing a specific role of Y925E-FAK in mediating enhanced protrusion.

Phosphorylation at Tyr-925 activates Rac1 via phosphorylation of p130^{CAS}

The current model implicates the Rac signaling pathway in leading edge protrusion via activation of the Arp2/3 complex to promote actin polymerization. Hence we hypothesized that the increase in cell protrusions that is seen in Y925E-FAK cells may be due to activation of Rac. To test this hypothesis, a G-LISA Rac activation assay was carried out on fibronectin-stimulated FAK, Y925F-FAK, and Y925E-FAK cells. Our results showed a significant increase in Rac activity (~26%) in Y925E-FAK cells compared with wild-type FAK cells (Figure 8A). A reduction in Rac activity was observed in Y925F-FAK cells, although not significant compared with that of wild-type FAK cells. Because Rac-dependent protrusion has been linked to phosphorylation of p130^{CAS}, which then binds to Crk and activates the signaling pathway involving the complex formation with Dock180/ELMO1 (Grimsley *et al.*, 2004; El-Sibai *et al.*, 2008; Sharma and Mayer, 2008), we first looked at Dock180/Rac interactions by coimmunoprecipitation assays. We noted an important decrease in Dock180/Rac1 interaction in Y925F-FAK cells compared with wild-type FAK cells and Y925E-FAK cells (Figure 8B). Second, quantification of Western blots revealed a significant 32% increase in phosphorylated p130^{CAS} in Y925E-FAK cells compared with wild-type FAK cells (Figure 8C). Inversely, Y925F-FAK cells exhibited a 44% decrease in phosphorylated p130^{CAS} compared with wild-type FAK cells. Immunolabeling of p130^{CAS} in wild-type FAK, Y925F-FAK, and Y925E-FAK cells showed localization of p130^{CAS} in FAs and colocalization of p130^{CAS} with wild-type and mutants of FAK (Figure 8D). Taken together, these data indicate that phosphorylation of FAK at Tyr-925 correlates with activation of Rac1 as well as an increased

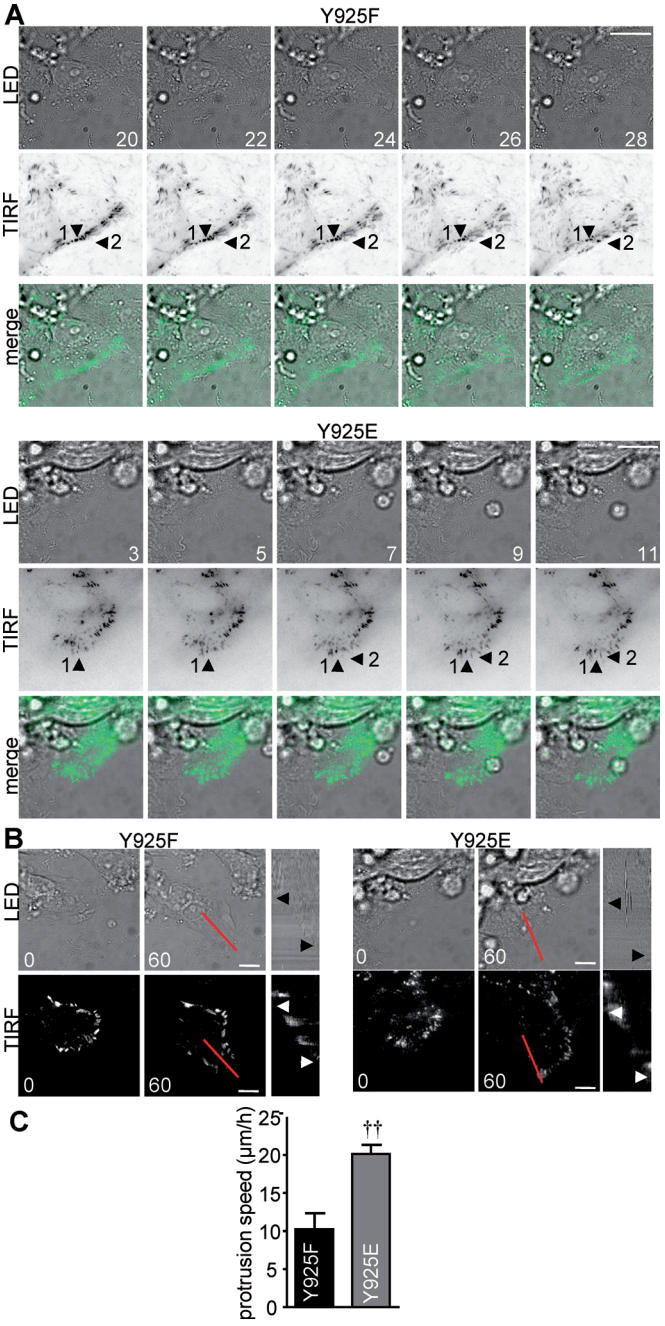

FIGURE 7: Increased cell protrusion in MEFs expressing Y925E-FAK. (A) Selected frames from the time-lapse sequence (1 frame per 30 s for a 30-min period) show representative images (at 2-min intervals) of spreading Y925F-FAK and Y925E-FAK cells. LED and TIRF images are shown in gray scale; Y925F-FAK and Y925E-FAK are shown in green in the merged images that correspond to the superimposition of LED and TIRF images of Y925F-FAK and Y925E-FAK cells. In Y925F cells, arrowheads point to FAs present at the cell leading edge in the process of disassembling (arrowhead 1) when new FAs assemble (arrowheads 2). In Y925E cells, arrowhead 1 points to an assembling FA, which starts to disassemble as a new FA assembles at its front (arrowhead 2). Scale bar, 10 μm. (B) Kymographs were generated on both TIRF and bright-field transmission images along the red lines using ImageJ software. (C) Cell protrusion speed was deduced from the kymographs. Note the significant difference in protrusion progression in Y925E-FAK cells compared with Y925F-FAK cells. $^{††}p < 0.01$. Scale bar, 5 μm.

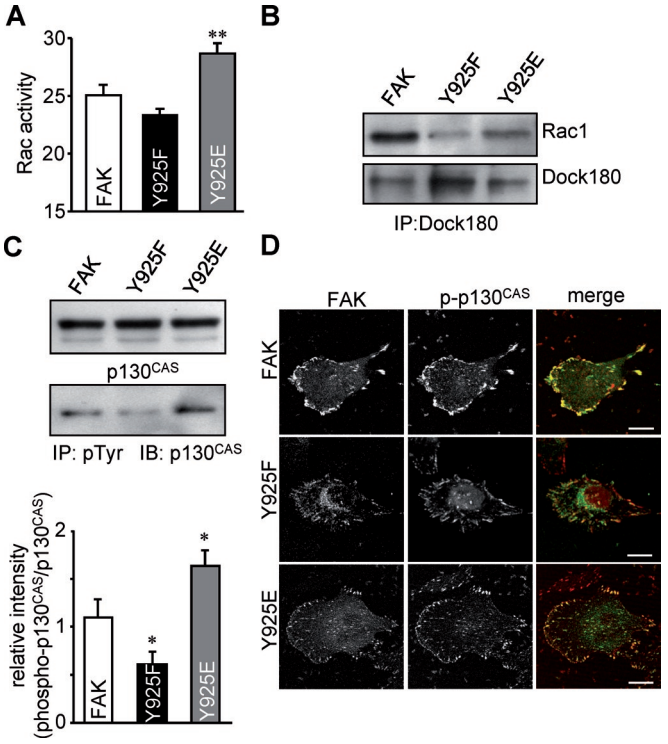

FIGURE 8: Increased phosphorylation of p130^{CAS} and Rac1 activation in Y925E-FAK cells. (A) Increased Rac1 activity in Y925E-FAK cells compared with wild-type FAK and Y925F-FAK cells. Cells were serum starved for 24 h before stimulation by fibronectin for 30 min. Rac activation was measured by G-LISA, and absorbance was read at 490 nm. Graph combines data from four experiments performed independently. (B) Cell extracts were immunoprecipitated using anti-Dock180 antibody and blotted for Rac1. Membranes were stripped and verified for Dock180 expression. (C) Equal expression levels of p130^{CAS} in wild-type FAK, Y925F-FAK, and Y925E-FAK cells. Phosphorylated p130^{CAS} was determined by immunoprecipitating phosphorylated proteins with an anti-phosphotyrosine antibody followed by blotting with a p130^{CAS} antibody. Mean phospho-p130^{CAS} data (mean ± SEM; n = 3 independent experiments). (D). Confocal images from fixed cells; YCam-tagged wild-type or mutant FAK (green) and immunostaining for phospho-p130^{CAS} (red); merged images (right). Scale bar, 10 μm.

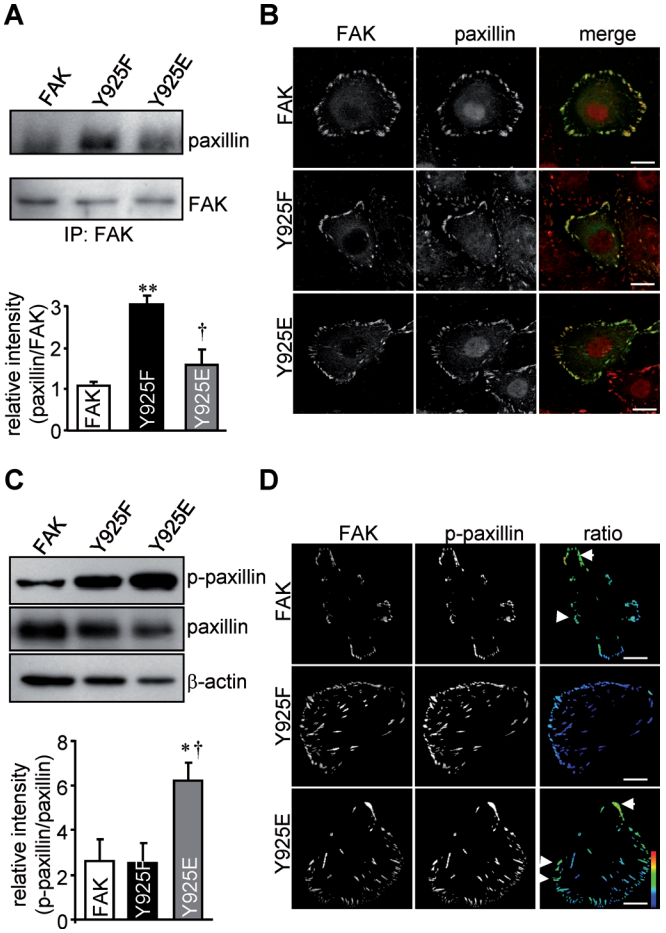

FIGURE 9: (A) Wild-type FAK, Y925F-FAK, and Y925E-FAK were immunoprecipitated using anti–C-terminal FAK antibody and blotted for paxillin. Membranes were stripped and blotted for FAK to control for equivalent expression of FAK. Mean data ± SEM (n = 3 independent experiments). **p < 0.0006 vs. FAK, and †p < 0.015 vs. Y925F-FAK. (B) Confocal images from fixed cells expressing wild-type or mutant FAK (green) and immunostained for paxillin (red). Scale bar, 10 μm. (C) Western blots showing phosphorylation status of paxillin at Tyr-118 in wild-type FAK, Y925F-FAK, and Y925E-FAK cells. Graph shows increased paxillin phosphorylation in Y925E-FAK cells compared with wild-type FAK cells (*p < 0.02) and to Y925F-FAK cells (†p < 0.02); n = 4 independent experiments. (D) Images were acquired on the Leica DMIRE2 microscope. Images were segmented and p-paxillin/FAK intensity ratios were calculated using Arivis Browser. Intensity ratios are scaled according to the spectrum table, which varies from 0.5 (blue) to 5.5 (red).

phosphorylation of p130^{CAS}. Combined with our observation that nonphosphorylatable Y925F-FAK–expressing cells display reduced association between Rac1 and Dock180, these data strongly suggest that FAK acts at least in part via the p130^{CAS}/Dock180/Rac1 signaling pathway to regulate cell protrusion activities.

Y925F-FAK interacts with nonphosphorylated paxillin

Previous reports have suggested that phosphorylation of FAK at Tyr-925 may be the mechanism used to induce FAK departure from the FA, via disruption of FAK/paxillin interactions, thus causing disassembly of FA. Coimmunoprecipitation experiments revealed a threefold increase in FAK association with paxillin in Y925F-FAK cells when compared with wild-type FAK or Y925E-FAK cells (Figure 9A). Of note, the difference in FAK/paxillin interaction between Y925E-FAK and wild-type FAK is not significant. Immunofluorescence labeling of MEFs expressing Y925F-FAK or Y925E-FAK showed localization of both FAK mutants to FAs, demonstrating that their recruitment to FAs by paxillin was not altered, as shown by merged signals of FAK with paxillin (Figure 9B). These results substantiate the fact that phosphorylation of Tyr-925 is not essential in the targeting of FAK to FAs. Because phosphorylation of paxillin has been implicated in adhesion turnover, we sought to investigate whether phosphorylation at Tyr-925 impacted paxillin phosphorylation. Western blot analysis using a phosphospecific antibody targeting paxillin phosphorylated at Tyr-118 revealed a 2.3-fold increase in phosphorylated paxillin for Y925E-FAK cells compared with wild-type FAK or Y925F-FAK cells (Figure 9C). Concomitantly, MEF cells were immunolabeled with the same phosphospecific paxillin (Figure 9D). In agreement with these results, analysis of intensity ratios of phospho-paxillin over FAK in wild-type or mutant FAK–expressed cells showed a lower ratio at FAs in Y925F-FAK cells than in wild-type FAK– or Y925E-FAK–expressing cells. Moreover, enrichment of phospho-paxillin was observed at disassembling FAs at the cell trailing edge (shown by an arrow) as well as in highly dynamic structures such as membrane protrusion (indicated by arrowheads).

Taken together, these results suggest an essential role of FAK phosphorylation at Tyr-925 in the regulation of FAK/paxillin interactions via control of paxillin phosphorylation, which leads to finer regulation of FA dynamics.

DISCUSSION

During migration, FAK is involved in both FA disassembly and cell protrusion, but the molecular mechanisms by which FAK coordinates these two processes remain poorly understood. In this study, we demonstrate that the outcome of FAK activity is dependent on its phosphorylation at Tyr-925. Using mutated forms of FAK at Tyr-925, we observed that impaired Tyr-925 phosphorylation decreases FA disassembly rate and reduces migration, whereas constitutive Tyr-925 phosphorylation increases dynamics of FAs at leading edges and enhances cell protrusion. We also found that the Tyr-925 phosphorylation status influences the FAK/paxillin interaction and activation of the $p130^{CAS}$–Rac pathway. Our work shows that FAK is involved in both regulating the disassembly of mature FA and cellular protrusion areas where nascent FAs are located. Interestingly other FA proteins such as Src and zyxin have been shown to shuttle between different subcellular locations (Hamadi *et al.*, 2009; Welman *et al.*, 2010). An exciting possibility would be that FAK could also shuttle between nascent and mature FAs. Determining whether such an exchange could carry information to regulate cell protrusion will promise important insights on the function of FAK as a molecular switch.

Regulation of FA disassembly and cell migration by FAK phosphorylation

Directional cell migration requires spatiotemporal control of FA formation and dissociation. Here we show that phosphorylation of FAK at Tyr-925 is necessary for efficient disassembly of FAs based on the decreased FA disassembly rate and the increased percentage of stable FAs in Y925F-FAK cells (Figure 4). This impaired disassembly led to a reduction in cell retractile activity (Figure 5) and consequently a decrease in migration speed (Figure 2). The mechanism implicated in these processes clearly involves FAK dynamics at FAs, as indicated by our FRAP studies (Figure 3). Increased FAK turnover at FAs led to the apparent stabilization of FAs, as already reported (Giannone *et al.*, 2004; Hamadi *et al.*, 2005). This decrease in FAK time residency may alter recruitment of crucial effectors at FAs essential for FA disassembly. Among them, proteases like calpain or guanine nucleotide exchange factors and GTPase-activating proteins might be involved (Carragher *et al.*, 2003; Iwanicki *et al.*, 2008).Our results are consistent with several studies reporting that phosphorylation of FAK is associated with FA disassembly and thus regulates cell migration (Sieg *et al.*, 1999; Carragher *et al.*, 2001; Giannone *et al.*, 2002; Westhoff *et al.*, 2004).

Regulation of FA disassembly by FAK/paxillin interactions

Our studies reveal an increased interaction between paxillin and the nonphosphorylatable form of FAK together with an increased association of phospho-paxillin with the phosphomimetic form of FAK. Moreover, in Y925E-FAK cells, an increased phospho-paxillin over FAK ratio was observed and enriched at both disassembling FAs at trailing edges and short-lived FAs at protrusions. This suggests that FAK phosphorylation is involved in paxillin phosphorylation, which in turn controls FAK/paxillin interactions, thereby participating in the regulation of FA dynamics. Previous structural studies indicated that phosphorylation of FAK at Tyr-925 may decrease paxillin binding to FAK, presumably leading to removal of FAK from FAs and, ultimately, FA disassembly (Tachibana *et al.*, 1995; Hayashi *et al.*, 2002; Gao *et al.*, 2004). In agreement, our data reveal that lack of FAK phosphorylation at Tyr-925 increased FAK interaction with nonphosphorylated paxillin and impaired FAs disassembly. On the other hand, constitutive phosphorylation of FAK at Tyr-925 while increasing paxillin phosphorylation and interaction with FAK affected the rate of FA disassembly only slightly, suggesting that either normally occurring phosphorylation of this site is sufficient to drive this process or additional mechanisms are needed to enhance this process. Among them, mechanisms involved in phosphatase-mediated dephosphorylation of FAK could be implicated, as already demonstrated (Yu *et al.*, 1998; Chen and Chen, 2006). Moreover, our results, while highlighting the importance of FAK phosphorylation in the control of FAK/paxillin interactions, clearly show that FAK phosphorylation at Tyr-925 is not sufficient to block localization of FAK to FAs, as previously suggested (Dixon *et al.*, 2004).

Regulation of FAs at protrusions by FAK

Y925E-FAK cells display increased migration efficiency (Figure 2). Because this effect is not due to an altered FA disassembly rate (Figures 3 and 4), the question then is how to explain the increases in cell migration observed for Y925E-FAK and wild-type FAK cells. We noted a significant increase in the formation of new protrusions in Y925E-FAK cells while no differences were observed between wild-type FAK and Y925F-FAK cells (Figure 5). Using TIRF microscopy, we also identified highly dynamic adhesions at the leading edges of Y925E-FAK cells (Figure 6). Finally, using dual TIRF/LED microscopy, we noticed that an enhanced adhesion dynamic correlated with increased protrusion activity (Figure 7). Therefore we propose a model in which FAK signaling couples the dynamics of nascent adhesions to enhanced protrusion, thereby promoting cell migration. Several lines of evidence support this model. First, in agreement with our data, it has been reported that FAK is required for formation of lamellipodia during cell spreading and migration into a wound (Tilghman *et al.*, 2005). Second, during migration, the effect of actin polymerization on protrusion is counterbalanced by the retrograde flow of actin that therefore regulates the net protrusion rate. The clutch hypothesis stipulates that integrin–actin linkage via the FA compartment inhibits actin retrograde flow by creating traction forces on the substratum (Mitchison and Kirschner, 1988); thus clutch engagement should result in enhanced protrusion. Indeed, a high correlation has been found between protrusion rate, actin dynamics, and FA assembly (Gupton and Waterman-Storer, 2006; Choi *et al.*, 2008). Moreover, formation of nascent adhesions appears to control the retrograde flow of actin (Alexandrova *et al.*, 2008). Taking these studies into account, our results are consistent with Tyr-925 phosphorylation participating in the molecular mechanisms involved in clutch engagement, thereby coupling nascent adhesion dynamics to protrusion.

Regulation of the $p130^{CAS}$/Rac1 pathway by FAK

What is the mechanism involved in enhanced FA dynamics and associated protrusion observed in Y925E-FAK cells? The best characterized downstream signaling pathway of FAK phosphorylation at Tyr-925 involves binding of Grb2 to phosphorylated FAK and subsequent activation of the ERK/MLCK pathway. However, the ability of Grb2 to bind to FAK as well as the level of MLC phosphorylation was not different in Y925E-FAK cells as compared with wild-type FAK and Y925F cells, suggesting that this pathway does not regulate protrusion and FA-associated dynamics in our cells as already reported for KM12C cells (Brunton *et al.*, 2005). On the other hand, we observed activation of $p130^{CAS}$ and subsequent increased Rac1 activity in Y925E-FAK cells as compared with FAK and Y925F-FAK

cells (Figure 8). This is mediated at least in part through increased Rac1/Dock 180 interactions. Moreover, it has been reported in NIH-3T3 cells that the interaction of $p130^{CAS}$ with FAK is decreased in Y861F-transfected cells during spreading, suggesting that phosphorylation of FAK at Tyr-861 is required for FAK/$p130^{CAS}$ interaction and activation of Rac downstream of the $p130^{CAS}$–Crk complex (Lim *et al.*, 2004). Conversely, in Y925E-FAK cells, FAK phosphorylation at Tyr-861 was increased by 3.5-fold as compared with FAK (Figure 1C), demonstrating that this mechanism is sufficient for activating the $p130^{CAS}$/Rac1 pathway. Rac activation together with increased FA turnover and lamellipodial protrusion is in agreement with a previous report, suggesting that the relationship between adhesion dynamics and protrusion is mediated by Rac activation (Schwartz and Horwitz, 2006). Indeed, activated Rac1 promotes formation of lamellipodia, membrane ruffling, and actin reorganization, events associated with cell migration (Hall, 2005; Guo *et al.*, 2006). Likewise, the $p130^{CAS}$/Rac1 pathway has been implicated in lamellipodia and invadopodia formation, and thus in mechanisms underlying cell invasion (Hsia *et al.*, 2003).

Overall, our findings provide new insights into the molecular mechanisms regulated by FAK that promote tumor cell migration. Activation of the positive FAK–Src feedback loop in tumor cells and subsequent phosphorylation of FAK at Tyr-925 likely play pivotal roles in cell migration and invasion by controlling FA turnover as well as lamellipodia formation. We propose that specifically targeting phosphorylation at Tyr-925 of FAK may provide a compelling basis for new therapeutic strategies.

MATERIALS AND METHODS

Reagents and antibodies

DMEM, Alexa Fluor 488–conjugated goat anti-mouse immunoglobulin (Ig) G, and Lipofectamine 2000 were obtained from Invitrogen (Paisley, UK). Fetal bovine serum (FBS), penicillin, streptomycin, and trypsin-EDTA solution were from Lonza (Verviers, Belgium). Western blot stripping reagent was from Millipore (Molsheim, France). Human fibronectin, mouse monoclonal FAK kinase (directed against amino acids 354–533), mouse monoclonal phospho-paxillin (Y118), and mouse monoclonal $p130^{CAS}$ antibodies were from BD Biosciences (Franklin Lakes, NJ). Rabbit anti–phospho-Y925 FAK antibody was from US Biological (Swampscott, MA). Rabbit anti–FAK C-terminal domain (amino acids 748–1052) and conformation-specific mouse monoclonal FAK (clone 2A7) antibodies were from Millipore (Molsheim, France). Mouse monoclonal anti-paxillin, rabbit polyclonal anti–phospho-Y397 FAK, rabbit anti–phospho-Y576 FAK, and rabbit anti–phospho-Y861 FAK antibodies were from Invitrogen. Mouse monoclonal anti–β-actin antibody was from Sigma (Lyon, France). Mouse monoclonal anti-phosphotyrosine (4G10 Platinum) and mouse monoclonal anti-Rac1 antibodies were from Millipore (Molsheim, France). Horseradish peroxidase–conjugated goat anti–mouse or anti–rabbit IgG were from Promega (Madison, WI). Goat polyclonal anti-Dock180 (N-ter) and horseradish peroxidase–conjugated rabbit anti–goat IgG were from Santa Cruz Biotechnology (Santa Cruz, CA). Rhodamine Red-X–conjugated goat anti–mouse or anti–rabbit antibodies were from the Jackson Laboratory (Bar Harbor, ME).

Expression vectors

pcDNA3.1-FAK/YCam expressing human FAK (wild-type FAK) fused to cyan fluorescent protein and YFP tags was constructed as described previously (Giannone *et al.*, 2002). The Y925F-FAK and Y925E-FAK mutants were generated using the QuikChange Mutagenesis kit (Agilent, Massy, France). Briefly, pcDNA3.1-FAK/YCam was used as a template to generate the Y925E-FAK construct using AKY925E (5′-GTCGAATGATAAGGTGGAAGAGAATGTGACGGGC-3′) and AKY925EAS (5′-GCCCGTCACATTCTCTTCCACCTTATCATTCGAC-3′) primers. The Y925F-FAK construct was made using AKY925F (5′-GTCGAATGATAAGGTGTTCGAGAATGTGACGGGC-3′) and AKY925FAS (5′-GCCCGTCACATTCTCGAACACCTTATCATTCGAC-3′) primers. pcDNA3.1-mCherry/Src-Y530F was generated by inserting the PCR product mCherry-Src-Y530F in pcDNA3.1(zeo) plasmid (Invitrogen) (Hamadi *et al.*, 2010). All constructs were amplified and purified using either Jetstar or Qiagen HiSpeed Maxiprep kits (Courtaboeuf, France) and specific point mutations were verified by sequencing. Plasmid enhanced green fluorescent protein/cherry-vinculin was kindly provided by I. Lavelin (Weizmann Institute of Science, Rehovot, Israel) (Wolfenson *et al.*, 2009).

Cell line, transfection, and fibronectin stimulation

Primary $FAK^{-/-}$ MEFs (passages 9–15) were maintained in DMEM supplemented with 10% FBS, 100 U/ml penicillin, and 100 μg/ml streptomycin as previously described (Neff *et al.*, 2003). Cells were maintained in a 5% CO_2 humidified incubator at 37°C. Transient transfections were used in all experiments because $FAK^{-/-}$ MEFs cells and our expression vectors both enclosed the neomycin resistance gene. To generate populations of MEFs expressing wild-type or mutant FAK, cells were seeded in 6-well plates and, after 24 h, transfected using Lipofectamine 2000 (Invitrogen) according to the manufacturer's directions. Transfection efficiency was 30–40% and was routinely verified by measuring YFP fluorescence. All experiments using transfected cells were carried out within 48 h after transfection. For fibronectin stimulation, 48 h–transfected cells were serum starved for 24 h and cells were detached from culture dishes using trypsin-EDTA, seeded onto fibronectin precoated 10-cm culture dishes, and incubated for 30 min.

Rac activation assay

Rac activation (Rac1/2/3) was measured using the G-LISA Rac Activation Assay Kit (Cytoskeleton, Denver, CO) according to the manufacturer's instructions. Briefly, a Rac-GTP–binding protein is linked to the bottom wells of a 96-well plate. Active GTP-Rac in cell lysates will bind to the Rac-GTP–binding protein, while inactive GDP-Rac will not. MEFs serum starved for 24 h were fibronectin stimulated and then lysed on ice. After centrifugation, aliquots of protein lysates were snap frozen in liquid nitrogen and kept at −80°C. Negative and positive controls were obtained with lysis buffer or nonhydrolyzable Rac, respectively. Thawed samples were added to wells precoated with Rac-GTP–binding domain (p21 binding domain) and incubated for 45 min on ice, followed by addition of the antigen-presenting buffer for 2 min, incubation for 45 min with Rac primary antibody (diluted at 1:200), and incubation for 45 min with secondary anti–horseradish peroxidase–labeled antibody (1:100), with thorough washing with wash buffer between all steps. The signal was measured immediately after addition of the horseradish peroxidase detection reagent at 492 nm using a microplate reader (Labsystems iEMS Reader MF, Helsinki, Finland).

Cell lysis, immunoprecipitation, and immunoblotting

At 48 h after transfection, cells were rinsed twice with ice-cold phosphate-buffered saline (PBS) (pH 7.4) and lysed for 30 min on ice with ice-cold IP lysis buffer (150 mM NaCl, 1% Triton X-100, 1% Nonidet P-40, 50 mM Tris-HCl, pH 8.0, 10 mM NaF, 2 mM Na_3VO_4, and a protease inhibitor mixture tablet [Complete Mini; Roche,

Meylan, France]). Lysates were cleared by centrifugation and protein concentrations determined (Dc protein assay; Bio-Rad, Hercules, CA) using bovine serum albumin (BSA) as a standard. For immunoprecipitation, 500 µg cell lysates was incubated with specific antibody (at dilutions recommended by manufacturers) for 3 h at 4°C with continuous shaking. Protein G Sepharose beads (GE Healthcare, Orsay, France) were then added for overnight incubation. Beads were collected, washed three times with ice-cold radioimmunoprecipitation assay buffer (150 mM NaCl, 1% Triton X-100, 0.5% Na deoxycholate, 0.1% SDS, 50 mM Tris-HCl, pH 7.5, and a protease inhibitor mixture tablet), and then resuspended in Laemmli buffer. For Western blots, 20 µg protein lysates were resolved by SDS–10% PAGE and transferred to polyvinylidene difluoride membranes (Hybond-P; GE Healthcare, Orsay, France). Blocking of the membrane was done in 5% nonfat milk–TBST (10 mM Tris-HCl, pH 7.4, 150 mM NaCl, 0.1% Tween-20) for 1 h at room temperature before overnight incubation at 4°C with primary antibodies (diluted 1:1000 in 5% nonfat milk-TBST). After three washes with TBST, the membrane was incubated with corresponding horseradish peroxidase–conjugated secondary antibodies (1:20,000). Signals were assessed using enhanced chemiluminescence (ECL Plus; GE Healthcare) and BioMax MR films (Eastman Kodak).

Immunofluorescence microscopy

At 24 h after transfection, MEFs were plated at low density on 10 µg/ml fibronectin-coated imaging µ-Dishes (Ibidi, Martinsried, Germany). After 24 h incubation, cells were fixed with 4% paraformaldehyde (PFA) for 10 min, permeabilized in 0.1% Triton X-100 for 5 min, blocked in 1% BSA/PBS for 1 h, and incubated with primary antibodies diluted (1:300) in 1% BSA/PBS for 1 h at room temperature. After three washes with PBS, cells were incubated with rhodamine-conjugated donkey anti–mouse antibody (1:400) for 1 h, washed three times with PBS, and then observed using a confocal microscope (Bio-Rad 1024, Kr/Ar laser; Nikon (Champigny sur Marne, France) Eclipse TE300, 60× water-immersion CFI Plan-Fluor, numerical aperture [NA] 1.3 objective). Z-series stacks (0.2-µm steps) were collected using LaserSharp 2000 software. YFP and rhodamine were excited at 488 and 568 nm, respectively, and fluorescence was collected at 522 nm (green) and 585 nm (red). ImageJ 1.37v software was used for treatment and analysis of images.

For PFA-fixed cells labeled for phospho-paxillin, a Leica (Nanterre, France) DMIRE2 microscope (40× HCX PL APO [1.25 NA] objective) was used to acquire 16-bit images. Subsequently, images were segmented using ImageJ software, and intensity ratios of phospho-paxillin on FAK signals were obtained with Arivis Browser software (Rostock, Germany).

Live cell imaging, FRAP, and TIRF experiments

For cell migration assays, confluent cells plated on 10 µg/ml fibronectin-coated coverslips were wounded with a pipet tip and mounted in a Ludin Chamber (Life Imaging Services, Basel Switzerland). The cells were then placed at 37°C, 5% CO_2, on a Leica DMIRE2 microscope. Images were acquired with a 40× HCX PL APO (1.25 NA) objective every 10 min during 13 h and a Leica DC350FX CCD camera piloted by Leica FW4000 software. Expressing cells at the leading edge of the wound were initially located via the GFP signal and were subsequently followed only via phase contrast. Up to 13 different fields were sequentially recorded during each experiment using a Märzhäuser (Wetzlar, Germany) automated stage piloted by the FW4000 software. The position of each cell was determined manually by tracking the center of the nucleus using MetaMorph (Molecular Devices, Sunnyvale, CA). Cell coordinates were exported to Microsoft Excel software to calculate all migration parameters. Live cell imaging for other experiments were carried out in phenol red–free medium supplemented with 20 mM HEPES and 10% FBS. Cells were maintained at 32°C using a temperature-controlled stage (Harvard apparatus). The 24 h–transfected cells were plated at low density on 10 µg/ml fibronectin-coated µ-Dishes. After 24 h incubation, images were acquired every 5 min for 1 h using a confocal microscope as above (488 nm excitation, 522 nm emission). Ratios of fluorescence at a FA at each time point (Ft) to that of the same FA at t = 0 (F0) were made. The rate of fluorescence loss was calculated by linear regression.

FRAP experiments were done on a Bio-Rad confocal microscope at 32°C. To avoid possible artifacts of overexpression, only cells expressing low but detectable amounts of protein were chosen for further analysis. Briefly, fluorescence intensity was measured at low laser power before bleach in selected regions of interest at FAs and in the cytosol. Photobleaching was done at 100% of the 488 nm line with four iterations. Recovery was followed with low laser power at various time intervals until the intensity had reached a steady plateau. For each time point, the intensity of the bleached area was normalized to that of a corresponding unbleached area. Fluorescence during recovery was normalized to the prebleached intensity. FRAP recovery curves were generated using GraphPad Prism 5 (La Jolla, CA).

TIRF images were acquired using an iMIC microscope (Till Photonics, Munich, Germany) equipped with a Cobolt Dual Calypso Laser 491/532 nm (Solna, Sweden) and an Olympus (Rungis, France) 60× TIRFM (1.45 NA) objective. During acquisition, cells were maintained at 37°C in a 5% CO_2 humidified atmosphere using an environmental control system (Life Imaging Services). TIRF images were acquired every 2 min on an EMCCD camera (Andor Technology, Belfast, Ireland) and analyzed using ImageJ software.

Image acquisition rate for bright-field transmitted LED/fluorescence microscopy was one frame per 30 s for 30 min. To estimate the velocity of cell protrusion, time-lapse images were analyzed using a kymograph macro of ImageJ software.

Protrusion–retraction analysis

Fluorescence time-lapse images of wild-type FAK, Y925F-FAK, and Y925E-FAK were used to outline cells by thresholding for pixels with high intensity. Areas covered by cells in consecutive images in the time series were subtracted to determine the percentage change of the total cell area contributing to protrusion or retraction occurring in the 2.5 min elapsed between images.

Statistical analysis

Data were analyzed using one-way analysis of variance and Student's *t* test, and differences were considered to be significant at $p \leq 0.05$. Unless otherwise stated, all data presented are from at least three independent experiments.

ACKNOWLEDGMENTS

This work was supported in part by grants from the Ligue Contre le Cancer (Comités Départementaux du Grand Est) to P. Rondé. A. Hamadi and K. Kolli were supported by doctoral fellowships from the Ministère de la Recherche and T. B. Deramaudt by a postdoctoral fellowship from the CNRS. We thank Romain Vauchelle and the Plateforme d'imagerie quantitative for technical assistance in data analyses. We thank R. Y. Tsien and B. Geiger for kindly providing us with the YCam and the cherry-vinculin vectors and D. Ilic for the $FAK^{-/-}$ cell line.

REFERENCES

Alexandrova AY, Arnold K, Schaub S, Vasiliev JM, Meister JJ, Bershadsky AD, Verkhovsky AB (2008). Comparative dynamics of retrograde actin flow and focal adhesions: formation of nascent adhesions triggers transition from fast to slow flow. PloS One 3, e3234.

Brunton VG, Avizienyte E, Fincham VJ, Serrels B, Metcalf CA III, Sawyer TK, Frame MC (2005). Identification of Src-specific phosphorylation site on focal adhesion kinase: dissection of the role of Src SH2 and catalytic functions and their consequences for tumor cell behavior. Cancer Res, 65, 1335–1342.

Calalb MB, Polte TR, Hanks SK (1995). Tyrosine phosphorylation of focal adhesion kinase at sites in the catalytic domain regulates kinase activity: a role for Src family kinases. Mol Cell Biol, 15, 954–963.

Calalb MB, Zhang X, Polte TR, Hanks SK (1996). Focal adhesion kinase tyrosine-861 is a major site of phosphorylation by Src. Biochem Biophys Res Commun 228, 662–668.

Carragher NO, Fincham VJ, Riley D, Frame MC (2001). Cleavage of focal adhesion kinase by different proteases during SRC-regulated transformation and apoptosis. Distinct roles for calpain and caspases. J Biol Chem 276, 4270–4275.

Carragher NO, Westhoff MA, Fincham VJ, Schaller MD, Frame MC (2003). A novel role for FAK as a protease-targeting adaptor protein: regulation by p42 ERK and Src. Curr Biol 13, 1442–1450.

Carter N, Nakamoto T, Hirai H, Hunter T (2002). EphrinA1-induced cytoskeletal re-organization requires FAK and $p130^{cas}$. Nat Cell Biol 4, 565–573.

Chen SY, Chen HC (2006). Direct interaction of focal adhesion kinase (FAK) with Met is required for FAK to promote hepatocyte growth factor-induced cell invasion. Mol Cell Biol 26, 5155–5167.

Cary LA, Han DC, Polte TR, Hanks SK, Guan JL (1998). Identification of $p130^{Cas}$ as a mediator of focal adhesion kinase–promoted cell migration. J Cell Biol 140, 211–221.

Chen SY, Chen HC (2006). Direct interaction of focal adhesion kinase (FAK) with Met is required for FAK to promote hepatocyte growth factor-induced cell invasion. Mol Cell Biol 26, 5155–5167.

Choi CK, Vicente-Manzanares M, Zareno J, Whitmore LA, Mogilner A, Horwitz AR (2008). Actin and α-actinin orchestrate the assembly and maturation of nascent adhesions in a myosin II motor-independent manner. Nat Cell Biol 10, 1039–1050.

Cooley MA, Broome JM, Ohngemach C, Romer LH, Schaller MD (2000). Paxillin binding is not the sole determinant of focal adhesion localization or dominant-negative activity of focal adhesion kinase/focal adhesion kinase-related nonkinase. Mol Biol Cell 11, 3247–3263.

Cooper LA, Shen TL, Guan JL (2003). Regulation of focal adhesion kinase by its amino-terminal domain through an autoinhibitory interaction. Mol Cell Biol 23, 8030–8041.

Dixon RD, Chen Y, Ding F, Khare SD, Prutzman KC, Schaller MD, Campbell SL, Dokholyan NV (2004). New insights into FAK signaling and localization based on detection of a FAT domain folding intermediate. Structure 12, 2161–2171.

El-Sibai M, Pertz O, Pang H, Yip SC, Lorenz M, Symons M, Condeelis JS, Hahn KM, Backer JM (2008). RhoA/ROCK-mediated switching between Cdc42- and Rac1-dependent protrusion in MTLn3 carcinoma cells. Exp Cell Res 314, 1540–1552.

Frame MC (2004). Newest findings on the oldest oncogene; how activated src does it. J Cell Sci 117, 989–998.

Gao G, Prutzman KC, King ML, Scheswohl DM, DeRose EF, London RE, Schaller MD, Campbell SL (2004). NMR solution structure of the focal adhesion targeting domain of focal adhesion kinase in complex with a paxillin LD peptide: evidence for a two-site binding model. J Biol Chem 279, 8441–8451.

Giannone G, Ronde P, Gaire M, Beaudouin J, Haiech J, Ellenberg J, Takeda K (2004). Calcium rises locally trigger focal adhesion disassembly and enhance residency of focal adhesion kinase at focal adhesions. J Biol Chem 279, 28715–28723.

Giannone G, Ronde P, Gaire M, Haiech J, Takeda K (2002). Calcium oscillations trigger focal adhesion disassembly in human U87 astrocytoma cells. J Biol Chem 277, 26364–26371.

Grande-Garcia A, Echarri A, de Rooij J, Alderson NB, Waterman-Storer CM, Valdivielso JM, del Pozo MA (2007). Caveolin-1 regulates cell polarization and directional migration through Src kinase and Rho GTPases. J Cell Biol 177, 683–694.

Grimsley CM, Kinchen JM, Tosello-Trampont AC, Brugnera E, Haney LB, Lu M, Chen Q, Klingele D, Hengartner MO, Ravichandran KS (2004). Dock180 and ELMO1 proteins cooperate to promote evolutionarily conserved Rac-dependent cell migration. J Biol Chem 279, 6087–6097.

Guinebault C, Payrastre B, Racaud-Sultan C, Mazarguil H, Breton M, Mauco G, Plantavid M, Chap H (1995). Integrin-dependent translocation of phosphoinositide 3-kinase to the cytoskeleton of thrombin-activated platelets involves specific interactions of p85α with actin filaments and focal adhesion kinase. J Cell Biol 129, 831–842.

Guo F, Debidda M, Yang L, Williams DA, Zheng Y (2006). Genetic deletion of Rac1 GTPase reveals its critical role in actin stress fiber formation and focal adhesion complex assembly. J Biol Chem 281, 18652–18659.

Gupton SL, Waterman-Storer CM (2006). Spatiotemporal feedback between actomyosin and focal-adhesion systems optimizes rapid cell migration. Cell 125, 1361–1374.

Hall A (2005). Rho GTPases and the control of cell behaviour. Biochem Soc Trans 33, 891–895.

Hamadi A, Bouali M, Dontenwill M, Stoeckel H, Takeda K, Ronde P (2005). Regulation of focal adhesion dynamics and disassembly by phosphorylation of FAK at tyrosine 397. J Cell Sci 118, 4415–4425.

Hamadi A, Deramaudt TB, Takeda K, Ronde P (2009). Src activation and translocation from focal adhesions to membrane ruffles contribute to formation of new adhesion sites. Cell Mol Life Sci 66, 324–338.

Hamadi A, Deramaudt TB, Takeda K, Ronde P (2010). Hyperphosphorylated FAK delocalizes from focal adhesions to membrane ruffles. J Oncol 2010, article 932803.

Harte MT, Hildebrand JD, Burnham MR, Bouton AH, Parsons JT (1996). $p130^{Cas}$, a substrate associated with v-Src and v-Crk, localizes to focal adhesions and binds to focal adhesion kinase. J Biol Chem 271, 13649–13655.

Hayashi I, Vuori K, Liddington RC (2002). The focal adhesion targeting (FAT) region of focal adhesion kinase is a four-helix bundle that binds paxillin. Nat Struct Biol 9, 101–106.

Hsia DA *et al.* (2003). Differential regulation of cell motility and invasion by FAK. J Cell Biol 160, 753–767.

Ilic D, Furuta Y, Kanazawa S, Takeda N, Sobue K, Nakatsuji N, Nomura S, Fujimoto J, Okada M, Yamamoto T (1995). Reduced cell motility and enhanced focal adhesion contact formation in cells from FAK-deficient mice. Nature 377, 539–544.

Iwanicki MP, Vomastek T, Tilghman RW, Martin KH, Banerjee J, Wedegaertner PB, Parsons JT (2008). FAK, PDZ-RhoGEF and ROCKII cooperate to regulate adhesion movement and trailing-edge retraction in fibroblasts. J Cell Sci 121, 895–905.

Kassenbrock CK, Anderson SM (2004). Regulation of ubiquitin protein ligase activity in c-Cbl by phosphorylation-induced conformational change and constitutive activation by tyrosine to glutamate point mutations. J Biol Chem 279, 28017–28027.

Lele TP, Thodeti CK, Pendse J, Ingber DE (2008). Investigating complexity of protein–protein interactions in focal adhesions. Biochem Biophys Res Commun 369, 929–934.

Lietha D, Cai X, Ceccarelli DF, Li Y, Schaller MD, Eck MJ (2007). Structural basis for the autoinhibition of focal adhesion kinase. Cell 129, 1177–1187.

Lim Y, Han I, Jeon J, Park H, Bahk YY, Oh ES (2004). Phosphorylation of focal adhesion kinase at tyrosine 861 is crucial for Ras transformation of fibroblasts. J Biol Chem 279, 29060–29065.

Liu Y, Loijens JC, Martin KH, Karginov AV, Parsons JT (2002). The association of ASAP1, an ADP ribosylation factor-GTPase activating protein, with focal adhesion kinase contributes to the process of focal adhesion assembly. Mol Biol Cell 13, 2147–2156.

McLean GW, Carragher NO, Avizienyte E, Evans J, Brunton VG, Frame MC (2005). The role of focal-adhesion kinase in cancer—a new therapeutic opportunity. Nat Rev Cancer 5, 505–515.

Millon-Fremillon A, Bouvard D, Grichine A, Manet-Dupe S, Block MR, Albiges-Rizo C (2008). Cell adaptive response to extracellular matrix density is controlled by ICAP-1–dependent β_1-integrin affinity. J Cell Biol 180, 427–441.

Mitchison T, Kirschner M (1988). Cytoskeletal dynamics and nerve growth. Neuron 1, 761–772.

Mohl C, Kirchgessner N, Schafer C, Kupper K, Born S, Diez G, Goldmann WH, Merkel R, Hoffmann B (2009). Becoming stable and strong: the interplay between vinculin exchange dynamics and adhesion strength during adhesion site maturation. Cell Motil Cytoskeleton 66, 350–364.

Neff L, Zeisel M, Druet V, Takeda K, Klein JP, Sibilia J, Wachsmann D (2003). ERK 1/2- and JNKs-dependent synthesis of interleukins 6 and 8 by fibroblast-like synoviocytes stimulated with protein I/II, a modulin from oral streptococci, requires focal adhesion kinase. J Biol Chem 278, 27721–27728.

Parsons JT (2003). Focal adhesion kinase: the first ten years. J Cell Sci 116, 1409–1416.

Pasapera AM, Schneider IC, Rericha E, Schlaepfer DD, Waterman CM (2010). Myosin II activity regulates vinculin recruitment to focal adhesions through FAK-mediated paxillin phosphorylation. J Cell Bio 188, 877–890.

Potter MD, Barbero S, Cheresh DA (2005). Tyrosine phosphorylation of VE-cadherin prevents binding of p120- and β-catenin and maintains the cellular mesenchymal state. J Biol Chem 280, 31906–31912.

Prutzman KC, Gao G, King ML, Iyer VV, Mueller GA, Schaller MD, Campbell SL (2004). The focal adhesion targeting domain of focal adhesion kinase contains a hinge region that modulates tyrosine 926 phosphorylation. Structure 12, 881–891.

Schaller MD, Hildebrand JD, Shannon JD, Fox JW, Vines RR, Parsons JT (1994). Autophosphorylation of the focal adhesion kinase, pp125FAK, directs SH2-dependent binding of pp60src. Mol Cell Biol 14, 1680–1688.

Schaller MD, Parsons JT (1995). pp125FAK-dependent tyrosine phosphorylation of paxillin creates a high-affinity binding site for Crk. Mol Cell Biol 15, 2635–2645.

Schlaepfer DD, Hanks SK, Hunter T, Van Der Geer P (1994). Integrin-mediated signal transduction linked to Ras pathway by GRB2 binding to focal adhesion kinase. Nature 372, 786–791.

Schlaepfer DD, Hunter T (1996). Evidence for in vivo phosphorylation of the Grb2 SH2-domain binding site on focal adhesion kinase by Src-family protein-tyrosine kinases. Mol Cell Biol 16, 5623–5633.

Schlaepfer DD, Mitra SK (2004). Multiple connections link FAK to cell motility and invasion. Curr Opin Genet Dev 14, 92–101.

Schober M, Raghavan S, Nikolova M, Polak L, Pasolli HA, Beggs HE, Reichardt LF, Fuchs E (2007). Focal adhesion kinase modulates tension signaling to control actin and focal adhesion dynamics. J Cell Bio 176, 667–680.

Schwartz MA, Horwitz AR (2006). Integrating adhesion, protrusion, and contraction during cell migration. Cell 125, 1223–1225.

Serrels B, Serrels A, Brunton VG, Holt M, McLean GW, Gray CH, Jones GE, Frame MC (2007). Focal adhesion kinase controls actin assembly via a FERM-mediated interaction with the Arp2/3 complex. Nat Cell Biol 9, 1046–1056.

Sharma A, Mayer BJ (2008). Phosphorylation of p130Cas initiates Rac activation and membrane ruffling. BMC Cell Biol 9, 50.

Sieg DJ, Hauck CR, Ilic D, Klingbeil CK, Schaefer E, Damsky CH, Schlaepfer DD (2000). FAK integrates growth-factor and integrin signals to promote cell migration. Nat Cell Biol 2, 249–256.

Sieg DJ, Hauck CR, Schlaepfer DD (1999). Required role of focal adhesion kinase, (FAK) for integrin-stimulated cell migration. J Cell Sci 112, 2677–2691.

Tachibana K, Sato T, D'Avirro N, Morimoto C (1995). Direct association of pp125FAK with paxillin, the focal adhesion-targeting mechanism of pp125FAK. J Exp Med 182, 1089–1099.

Tachibana K, Urano T, Fujita H, Ohashi Y, Kamiguchi K, Iwata S, Hirai H, Morimoto C (1997). Tyrosine phosphorylation of Crk-associated substrates by focal adhesion kinase. A putative mechanism for the integrin-mediated tyrosine phosphorylation of Crk-associated substrates. J Biol Chem 272, 29083–29090.

Tilghman RW, Slack-Davis JK, Sergina N, Martin KH, Iwanicki M, Hershey ED, Beggs HE, Reichardt LF, Parsons JT (2005). Focal adhesion kinase is required for the spatial organization of the leading edge in migrating cells. J Cell Sci 118, 2613–2623.

Tomar A, Wang Y, Kumar N, George S, Ceacareanu B, Hassid A, Chapman KE, Aryal AM, Waters CM, Khurana S (2004). Regulation of cell motility by tyrosine phosphorylated villin. Mol Biol Cell 15, 4807–4817.

Volberg T, Romer L, Zamir E, Geiger B (2001). pp60(c-src) and related tyrosine kinases: a role in the assembly and reorganization of matrix adhesions. J Cell Sci 114, 2279–2289.

Webb DJ, Donais K, Whitmore LA, Thomas SM, Turner CE, Parsons JT, Horwitz AF (2004). FAK–Src signalling through paxillin, ERK and MLCK regulates adhesion disassembly. Nat Cell Biol 6, 154–161.

Welman A, Serrels A, Brunton VG, Ditzel M, Frame MC (2010). A two color photoactivatable probe for selective tracking of proteins and cells. J Biol Chem.

Westhoff MA, Serrels B, Fincham VJ, Frame MC, Carragher NO (2004). SRC-mediated phosphorylation of focal adhesion kinase couples actin and adhesion dynamics to survival signaling. Mol Cell Biol 24, 8113–8133.

Wolfenson H, Lubelski A, Regev T, Klafter J, Henis YI, Geiger B (2009). A role for the juxtamembrane cytoplasm in the molecular dynamics of focal adhesions. PloS One 4, e4304.

Yu DH, Qu CK, Henegariu O, Lu X, Feng GS (1998). Protein-tyrosine phosphatase Shp-2 regulates cell spreading, migration, and focal adhesion. J Biol Chem 273, 21125–21131.

Zaidel-Bar R, Ballestrem C, Kam Z, Geiger B (2003). Early molecular events in the assembly of matrix adhesions at the leading edge of migrating cells. J Cell Sci 116, 4605–4613.

Zaidel-Bar R, Itzkovitz S, Ma'ayan A, Iyengar R, Geiger B (2007a). Functional atlas of the integrin adhesome. Nat Cell Biol 9, 858–867.

Zaidel-Bar R, Milo R, Kam Z, Geiger B (2007b). A paxillin tyrosine phosphorylation switch regulates the assembly and form of cell-matrix adhesions. J Cell Sci 120, 137–148.